A Computer Simulation of Free-Volume Distributions and Related Structural Properties in a Model Lipid Bilayer

Tian-xiang Xiang

Department of Pharmaceutics and Pharmaceutical Chemistry, University of Utah, Salt Lake City, Utah 84112 USA

ABSTRACT   A novel combined approach of molecular dynamics (MD) and Monte Carlo simulations is developed to calculate various free-volume distributions as a function of position in a lipid bilayer membrane at 323 K. The model bilayer consists of 2×100 chain molecules with each chain molecule having 15 carbon segments and one head group and subject to forces restricting bond stretching, bending, and torsional motions. At a surface density of 30 Å^2/chain molecule, the probability density of finding effective free volume available to spherical permeants displays a distribution with two exponential components. Both pre-exponential factors, p_1 and p_2, remain roughly constant in the highly ordered chain region with average values of 0.012 and 0.00039 Å^{-3}, respectively, and increase to 0.049 and 0.0067 Å^{-3} at the mid-plane. The first characteristic cavity size V_1 is only weakly dependent on position in the bilayer interior with an average value of 3.4 Å^3, while the second characteristic cavity size V_2 varies more dramatically from a plateau value of 12.9 Å^3 in the highly ordered chain region to 9.0 Å^3 in the center of the bilayer. The mean cavity shape is described in terms of a probability distribution for the angle at which the test permeant is in contact with one of and does not overlap with anyone of the chain segments in the bilayer. The results show that (a) free volume is elongated in the highly ordered chain region with its long axis normal to the bilayer interface approaching spherical symmetry in the center of the bilayer and (b) small free volume is more elongated than large free volume. The order and conformational structures relevant to the free-volume distributions are also examined. It is found that both overall and internal motions have comparable contributions to local disorder and couple strongly with each other, and the occurrence of kink defects has higher probability than predicted from an independent-transition model.

INTRODUCTION

The ability to predict transport behaviors of permeant molecules across biological membranes is a prerequisite for the analysis of many biological processes and for the design of various drug delivery systems. A fundamental component of biological membranes is lipid bilayers, in which molecular organization varies, on an atomic dimension, with distance from the interfaces. As a consequence, it is possible to observe partition and diffusion processes in a lipid bilayer as a function of position from the interface only if certain probe groups are attached to the chain molecules in the bilayer (Griffith et al., 1974; Windrem and Plachy, 1980), which, unfortunately, may disturb the local structure of the bilayer and thereby affect the transport processes. Furthermore, it is a subject of debate to use various physicochemical relationships obtained for bulk and polymeric systems to describe phenomena occurring in interfacial phases, in particular, in highly ordered alkyl chain domains in lipid bilayer membranes. Interest in permeation properties in the highly ordered chain regions is heightened by results from our recent experiments on transport across egg-lecithin planar lipid bilayers (Xiang et al., 1992), which strongly suggest that the transport barrier for nonelectrolyte molecules is located in the highly ordered chain region.

With the advance of modern computer technology and the emergence of various sophisticated potential energy functions, computer simulations have become a powerful means to gain detailed information about molecular struc-

tures and dynamic processes which can not be easily provided by conventional laboratory experiments. Although certain aspects of static and dynamic structures in lipid monolayers and bilayers have been studied by means of Monte Carlo (MC) (Milik et al., 1990, 1992), master equation (ME) (Ferrarini, 1989), Brownian dynamics (BD) (Pastor et al., 1988a, 1988b) and molecular dynamics (MD) (van der Ploeg and Berendsen, 1982, 1983; Egberts and Berendsen, 1988; Bareman and Klein, 1990; Biswas and Schurmann, 1991; Pastor et al., 1991; Karaborni and Toxvaerd, 1992) simulations, there is still a need to investigate those monolayer or bilayer properties that are closely related to the underlying partition and diffusion processes with physical parameters (e.g., surface density) comparable with experimental or physiological conditions. Studies of the effects of permeant's size (Stein, 1986; Walter and Gutknecht, 1986) and temperature (Vaz et al., 1985) on translational diffusion in lipid bilayers suggest that a free-volume model is appropriate for the description of diffusion processes in the bilayers. In the free-volume theory of Cohen and Turnbull (Cohen and Turnbull, 1959; Turnbull and Cohen, 1970), translational diffusion of a permeant occurs when statistical redistribution of free volume opens up a void of a critical size in the immediate vicinity of the permeant. The concept of free volume has also been utilized to describe the effects of molecular size and shape and medium density on partitioning of solutes into interphases as well as between simple liquids (Schnitzer, 1988; Eiteman and Gainer, 1989). Earlier, a molecular theory for the evolution of free volume in lipid bilayers was proposed by Träuble to explain relatively high permeability

for water and other small molecules (Träuble, 1971). However, a quantitative knowledge of free-volume distributions in lipid bilayers is still lacking. Questions fundamental to the application of the concept of free volume to transport processes in lipid bilayers include (a) how various free-volume distributions depend on location in the bilayer interior? (b) Which of the free-volume properties, the number of cavities and the mean cavity size, is the major determinant for the location of transport barrier in the bilayers? (c) What is the mean cavity geometry of free volume in the bilayers?

The primary objective of this study is to address these questions by calculating, for the first time, various free-volume distributions in a model bilayer as a function of position from the interface. The bilayer microstructures (i.e., atomic Cartesian coordinates) are obtained from a MD simulation in which various realistic interaction energies between chain segments are considered. In contrast to the more traditional MC method for the structural generation, the MD simulation is better suited to obtain bilayer structures with more precise conformational correlation. Cooperative torsional motions have been shown to be responsible for the creation and movement of relatively large cavities in lipid bilayers (Träuble, 1971) and to be correlated with diffusion processes in polymers. From the simulated bilayer microstructures, the free-volume distributions are calculated by means of a Monte-Carlo technique (Shah et al., 1989) and further examined with various analytical models. In the Monte-Carlo method, a number of points representing the positions of test permeants are randomly chosen in the bilayer and the number of permeants which do not overlap with any chain segment in the bilayer is counted as functions of permeant's size and location in the bilayer interior. The objectivity nature of the method is especially promising considering the ambiguity involved in the concept of free volume because of the irregularity of and the ill-defined boundary between the cavities. Other structural properties of the bilayer are also described. They include segmental order parameter, molecular orientation, and conformational statistics. The characteristic free-volume parameters and other simulation results are discussed in conjunction with available experimental data and theoretical models.

COMPUTATIONS

Molecular dynamics simulation

A relatively large bilayer assembly with 2×100 lipid molecules was simulated in order to avoid possible artificial structures as found in small bilayer assemblies (van der Ploeg and Berendsen, 1983) bilayer was confined in a unit box with periodic boundary conditions in the x-y domain. Each chain molecule had 14 methylene, one methyl, and one head group. The molecular model was similar to the flexible chain model employed in our previous molecular dynamics studies on

segmental relaxation of liquid hydrocarbons (Xiang et al., 1991; Liu et al., 1992), in which all groups were treated as single spheres and the following force field was used

$$V_{total} = \sum_{bonds} \frac{k_b}{2} (b - b_o)^2 + \sum_{angles} \frac{k_\theta}{2} (\cos \theta - \cos \theta_o)^2 \quad (1)$$

$$+ \sum_{dihedrals} V_{CCCC}(\cos \phi) + \sum_{i<j} 4\epsilon_{ij} \left[\left(\frac{\sigma_{ij}}{R_{ij}} \right)^{12} - \left(\frac{\sigma_{ij}}{R_{ij}} \right)^6 \right]$$

The bond lengths (b) and angles (θ) were allowed to vibrate near the equilibrium positions (b_o, θ_o) using appropriate harmonic forces. The frequency for bond stretch (C-C) was reduced by about three-fold in this simulation compared to the real frequencies observed in IR spectroscopy. Previous studies have shown that structural properties of hydrocarbon liquids including conformational structures are not seriously disturbed by the changes of vibrational frequencies for bond stretch (Helfand et al., 1980). It is superior, as noted by Helfand and Fixman (Helfand, 1979; Fixman, 1974), to the constraint method used by a number of authors, in which bond lengths are fixed. The Rychaert-Bellemans potential (Rychaert and Bellemans, 1975),

$$V_{CCCC}(\cos \phi) = (2.217 + 2.905 \cos \phi - 3.135 \cos^2 \phi$$

$$- 0.731 \cos^3 \phi + 6.27 \cos^4 \phi - 7.527 \cos^5 \phi) \quad (2)$$

$$(kcal/mol)$$

was used for torsional motions of the C-C-C-C linkages (ϕ). This potential energy function was derived originally from infrared spectroscopic studies (Scott and Scheraga, 1966; Woller and Garbisch, 1972) and has been tested by MD simulations of liquid hydrocarbons (Rychaert and Bellemans, 1975). A Lennard-Jones (12–6) potential was employed for intermolecular interactions and for interactions between segments separated by more than three bonds in the same molecule. The L-J parameters (σ, ϵ) were determined on the basis of the results given by Jorgensen and Tirado-Rives (1988), Weiner et al. (1984), and van der Ploeg and Berendsen (1982). Combination rules were used for cross interactions, and a cut-off radius of 13 Å was used for all the L-J interactions. The relevant geometric and force parameters are listed in Table 1.

Since our attention in this work is focused on the free-volume distributions in the alkyl chain region where the transport barrier for nonelectrolyte molecules resides (Xiang et al., 1992) and since an explicit modelling of head groups (e.g., phosphatidylcholine) and the neighboring water phase would require substantially more CPU time, a simple model was adopted for the head group and its interaction with the adjacent aqueous solution. In this model, the head group has the same size as a carboxylate group and is anchored to a mobile plane by a harmonic force. Similar strategies have been taken in other MD and BD simulations of model monolayers and bilayers (van der Ploeg and Berendsen, 1982, 1983; Pastor et al., 1988a, 1988b, 1991; Bareman and Klein,

TABLE 1   Geometrical and force parameters used in the simulation

	b_o	k_b	θ_o	k_θ	σ	ϵ
	Å	kJ/Å² mol	degrees	kJ/mol	Å	kJ/mol
C-C	1.54	9.3×10^2				
C-X*	1.54	9.3×10^2				
C-C-C			110	1.3×10^2		
C-C-X			110	1.3×10^2		
$CH_2 \cdots CH_2$					3.74	0.43
$CH_3 \cdots CH_3$					3.90	0.61
$X \cdots X$					4.22	0.92

* X denotes a carboxylate head group.

1990; Biswas and Schurmann, 1991; Karaborni and Toxvaerd, 1992). The force constant chosen ($k_i = 3.0 \text{ kJ/mol Å}^2$) is comparable with the one used in a statistical mechanical study of phase transitions in phospholipid bilayers (Jacobs et al., 1977). The "roughness" energy associated with this harmonic force arises from a dynamic balancing between the strong interaction of head groups with the bulk water and the hydrophobic interaction of alkyl chains when the segments are exposed to the water phase. The position of the mobile interfacial plane is defined as the average z coordinates of all the carboxylate groups in the same monolayer. It is determined primarily by interaction between chain molecules in different monolayers and by an external pressure exerted longitudinally on the head groups. One atmosphere was used in this work. To mimic the effect of the neighboring aqueous phase on segmental motion, a harmonic force (1.0 kJ/mol) was imposed on a segment whenever it moved outside the interfacial plane.

The MD simulation was performed on an IBM 3090 supercomputer. The equations of motion were integrated by using the Verlet algorithm (Allen and Tildesley, 1989) and a time step of 5 fs. This time step was one order of magnitude smaller than the reciprocal of the vibrational frequencies for the bond stretch. The box length was determined from a selected surface density. It was varied in our initial control simulations in the range of 20–35 Å²/chain molecule in order to find out an optimal surface density at which the segmental order parameters calculated are in best agreement with experimental values (vida supra). The simulation was divided into two phases. In the first phase, the equilibrium of the system was reached through a sufficiently long run (~100,000 time steps) starting from an all-*trans* configuration for all the chain molecules in the bilayer and was monitored by various order parameters, temperature, and other structural quantities. The segmental velocities were adjusted according to the Maxwell velocity distribution at a certain interval of time to give an average temperature of 323 K (Andrea et al., 1983). At equilibrium, the fluctuation of system temperature between temperature samplings was ± 4 K, and no significant drift of temperature was observed. The production phase consisted of 10 trajectory segments, each separated by 10,000 time steps. At the end of each segment run, the atomic coordinates were stored in files to be used for subsequent calculations.

We have also conducted an NVT MD simulation on liquid *n*-octane using the same potential functions and chain model.

The box length was varied until the system pressure including a long-range correction (Allen and Tildesley, 1989) was 3 ± 50 atm. As the isothermal compressibility for liquid *n*-octane is on the order of 1×10^{-4}/atm, the deviation of pressure from 1 atm creates an error of no greater than 0.1% for the total free-volume fraction.

Monte Carlo method

From the microstructure of the lipid bilayer as determined from the MD simulation, free volume available to spherical permeants with different diameters was evaluated using a Monte Carlo technique (Shah et al., 1989).

In this method, N (= 2×10^6) points representing the centers of the test permeants were randomly chosen within the central box. The bilayer was divided into 21 strips along the z direction. The width of each strip, Δz, was determined by the instantaneous thickness of the bilayer which is defined as the distance between the two mobile interfaces. The bilayer thickness averaged over 10 different bilayer microstructures was 30.0 ± 0.6 Å. A counter which corresponded to one of the strips was selected if the randomly generated point fell into the strip. 50 counters for that strip were then activated for permeants of different diameters d in the range of 0–8 Å. The maximum size of a sphere, d_m, that can be inserted without overlapping even partially with any van der Waals (vdW) pseudoatom in the lipid bilayer was obtained. The maximum diameter d_m is defined, as shown in Fig. 1, such that further increase of the diameter would cause the distance between the test permeant and the center of one of the pseudoatoms in the bilayer, say the jth segment, to become smaller than $r_{e,j} = (d_m + \sigma_j)/2^{5/6}$, where $r_{e,j}$ is the position of the minimum energy in the corresponding L-J (12–6) potential. All counters corresponding to diameters less than d_m were incremented by one, implying thereby that any spherical permeant with size less than d_m can occupy at that point. If N_i is the total number of points which fall into the ith strip ($i = 1, 2, \ldots, 21$) and $N_{i,d}$ is the number of points, among the N_i points, in the unoccupied volume at which a permeant of diameter d can be inserted, then the ratio of $N_{i,d}$ to N_i, $f(V, z) = N_{i,d}/N_i$, gives accumulated free-volume fraction at position z which is available to a spherical permeant with a vdW volume of $V \leq \pi d^3/6$, where z [= (i − 0.5)Δz] is the coordinate along the bilayer normal whose origin is located at one of the interfacial plane.
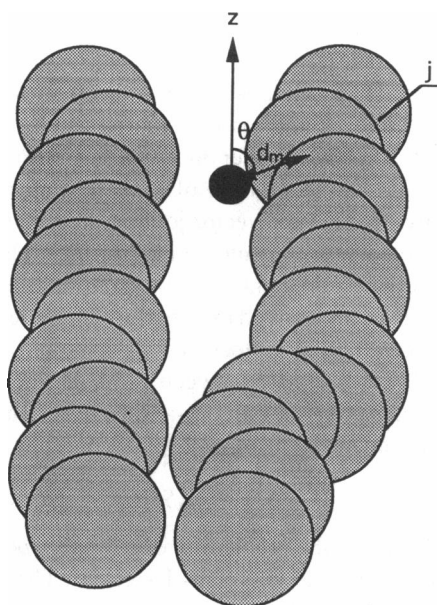
FIGURE 1   A schematic illustration of the definitions of the maximum diameter d_m of a test permeant and the contact angle θ between the test permeant and one of the chain segments which is in contact with the test permeant. Only portions of two surrounding chain molecules are drawn, in which one portion has an all-*trans* conformation, while the other has a kink $(g^+ tg^-)$ sequence.

The distributions of the accumulated free-volume fraction obtained were differentiated with respect to $-V$ to give the probability distributions of cavity sizes available to spherical permeants (*vida supra*). The resulting probability distributions were further analyzed by a curve-fitting program (MINSQ, Micromath Scientific Software, Salt Lake City, Utah). The most appropriate model was selected based on a modified Akaike Information Criterion, which is also known as the Model Selection Criterion (MSC). When comparing models with different numbers of parameters, this criterion places a burden on the model with more parameters. In addition, it is also independent of the scaling of the data points used. In our nonlinear regression analysis, the following quantity

$$\chi^2 = \sum_i \frac{[p(V_i, z) - P(V_i, z)]^2}{p^2(V_i, z)} \tag{3}$$

was minimized, where $p(V_i, z)$ and $P(V_i, z)$ are data points from our simulation results and from a theoretical model function, respectively. A weighing factor, $w_i = 1/p^2(V_i, z)$, was used as the variance of the accumulated free-volume fraction at V_i was assumed to be proportional to the square of the total count which falls into the given region.

The mean cavity geometry of the free volume in the bilayer is described by the probability distribution of the angle θ between the bilayer normal and the vector connecting the test permeant and one of the chain segments in the bilayer which is in contact with and has the shortest distance from the test permeant as defined above (cf. Fig. 1). For each bilayer region i and each volume interval V of the test permeant, 18

counters were set up, each corresponding to an angle strip between 0 and 180°. If the contact angle θ fell into one of the equally spaced strips, the counter associated with that angle strip, $N_{\theta,i,v}$, was incremented by one. The probability density for the contact angle θ is then calculated as $P(\theta, V, z) = N_{\theta,i,v}/N_{i,v}/\Delta\theta$, where $N_{i,v}$ is the total number of points which fall into the region (i, V) and $\Delta\theta$ is the increment of the angle strip.

Ten different microstructures of the model bilayer, each separated by ~10,000 time steps, were generated after the equilibrium of the system had been reached. $f(V, z)$, $P(\theta, V, z)$, and other structural quantities were calculated for each microstructure and arithmetic averages of the corresponding distributions were then obtained. As the bilayer structure is symmetric statistically with respect to the mid-plane, arithmetic averages of the free-volume distributions and other relevant structural properties in the regions of opposing monolayers which are symmetric with respect to the reflection about the mid-plane were also taken. The resulting quantities are presented in the following section.

RESULTS AND DISCUSSION

An instantaneous view of an equilibrium bilayer system at 323 K is shown in Fig. 2 along the y axis. Independent ^{2}H NMR experiments on bilayers of 1,2-dipalmitoyl-3-sn-phosphatidylcholine (DPPC) at 323 K gave a surface density of 30.5 Å^2/chain molecule, which varied only slightly with temperature above T_c (Seelig and Seelig, 1974; Schindler and Seelig, 1975). The surface density used in the present simulation is 30 Å^2/chain molecule, which is very close to the NMR data, but about 10% smaller than the one obtained from x-ray diffraction measurement (Rand and Parsegain, 1989). Apart from dramatic fluctuation in segmental positions, the frequent crossing of chain molecules over the mid-plane and the large wobbling motion of some chain molecules away from the bilayer normal are noted in Fig. 2.
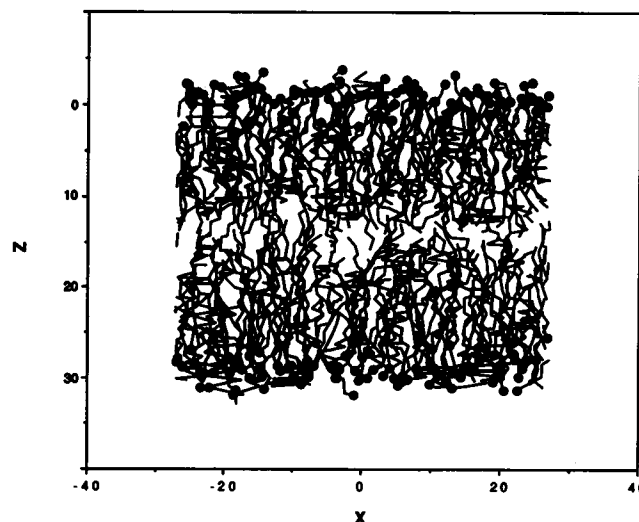

FIGURE 2   An instantaneous view of the bilayer system at 323 K and a surface density of 30 Å^2/chain molecule along y axis. Head groups are shown in black dots.

Segmental order parameter

Local chain structure has been investigated by deuterium quadruple resonance experiments on C-D bonds at different positions in DPPC multilayer vehicles (Seelig and Nieder-berger, 1974; Seelig and Seelig, 1974; Schindler and Seelig, 1975). Aside from a difference in the average orientation of segments close to the head groups, both chains in a DPPC molecule behave similarly in terms of local order and orientational distributions (De Loof et al., 1991). Thus, it is reasonable to compare, as shown in Fig. 3, the experimental C-D order parameters at different segmental positions (Seelig and Seelig, 1974) with those derived from the present MD simulation. The order parameter, S_{CD}, is defined as

$$S_{CD} = \frac{1}{2}\langle 3 \cos^2 \Theta - 1 \rangle \qquad (4)$$

where Θ is the angle between the C-D vector and the bilayer normal, and where the brackets represent an ensemble average. Referring to Fig. 3, both the simulation and the experimental results exhibit a highly ordered plateau region along the chain with a rapid decrease of the order parameter toward the chain tail. The apparent decrease in the order parameter at C_2 as contrast with the corresponding experimental value is expected given the fact that there are two chain molecules in a DPPC molecule which are covalently bonded to the same polar group. The pairing constraint anchors the chains to a narrower interfacial region than would be the case for single-chain molecules and may thereby inhibit their mobility and decrease the local free-volume fraction. Nevertheless, as suggested by the ^{2}H NMR measurements (Schindler and Seelig, 1975), such an effect, if it exists, is restricted to the few segments close to the head group and is no longer observable from C_3 onward. The general agreement of the calculated order parameters with the experimental values also serves as an evidence for the ad-

equacy of our model bilayer as a prototype for real lipid bilayer membranes.

It is important to understand the roles that overall reorientation and internal motion of chain molecules play in determining the local disorder in the bilayer (Peterson and Chan, 1977). Overall rotation of a chain molecule can be specified by defining the vector joining the first segment of the chain molecule to its center of mass as the molecular long axis. The order parameters due to overall and internal motions (S_O and S_I) are derived by substituting, respectively, the tilt angle between the molecular long axis and the bilayer normal (Θ') or the angle between the C-D vector and the molecular long axis (Θ'') into Eq. 4. If the overall and internal motions are independent of each other, one has

$$S_{CD} = S_O S_I. \qquad (5)$$

Fig. 4 illustrates the probability distribution, $p(\cos \Theta')$, of finding the tilt angle at Θ' versus $1 - \cos\Theta'$. The probability decreases rapidly as the tilt angle increases with an order parameter (S_O) of 0.64. The order parameter calculated from the independent model is shown in Fig. 3. A comparison of the relative magnitude of S_O and S_I reveals that both overall rotation and internal motion have comparable contributions to the overall order parameter S_{CD}. For the first four segments, the independent assumption gives the order parameter in close agreement with the true order parameter. The deviation becomes significant further down the chain, suggesting the occurrence of coupling between the overall and internal motions. The roughly constant gradient for the order parameter calculated from the independent model resembles the order parameter profile obtained from an ESR spin label measurement (Hubbell and MaConnell, 1971). In that experiment, the order parameter was primarily sensitive to internal motions because of the short time scale of the measurement. As a result, the observed order parameter might not reflect the coupling between the overall and internal motions. The coupling between overall and internal motions is entailed to avoid the swing of a chain molecule over a large volume. The replacement of sites occupied by other chain
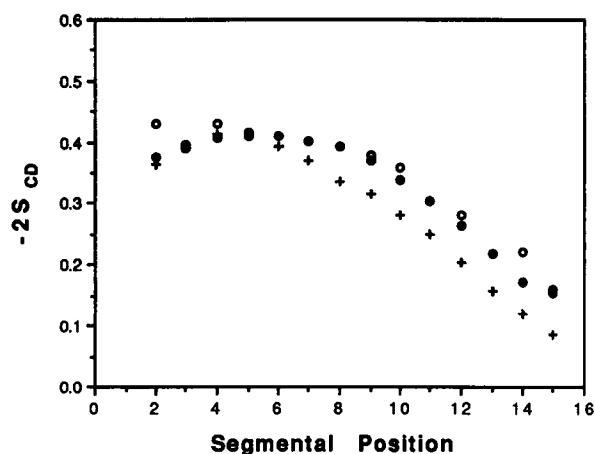

FIGURE 3 The C-D segmental order parameters at 323 K versus segmental position: ●, from the present MD simulation using Eq. 4 with a surface density of 30 Å²/chain molecule; ○, from the NMR experiment (Seelig and Seelig, 1974); and +, from the present MD simulation along with the assumption of independent motions for both overall and internal modes (cf., Eq. 5).
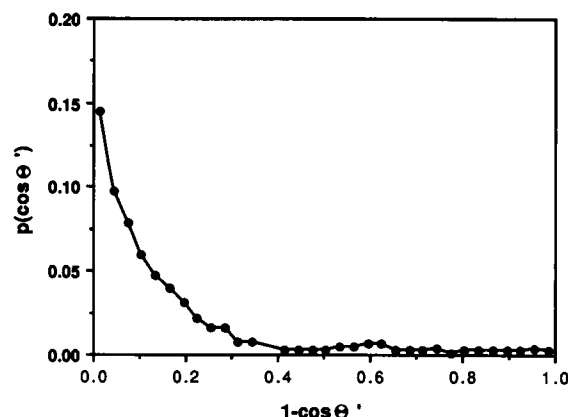

FIGURE 4 The probability distribution for the tilt angle Θ' as a function of $1 - \cos\Theta'$.

molecules requires a large amount of energy. For instance, the cohesion energy for a CH_2 group in a bilayer is about 1 kcal/mol (Vaz et al., 1979). Various coherent motions exist extensively in liquid hydrocarbons, in which several torsional transitions occur closely in space and time in such a way that essentially no new volume is created (Helfand, 1971; Skolnick and Helfand, 1980; Helfand, 1985; Xiang, et al., 1991). They can also preserve the chain orientation along the bilayer normal, giving the plateau order parameter along the chain.

Free-volume distributions

Fig. 5 shows two representative distributions of the accumulated free-volume fraction, $f(V, z)$, at $z = 1.50$ and 15.0 Å, respectively, as a function of the vdW volume of a spherical test permeant (V). The distributions in the region between 0.0 and 4.0 Å^3 are presented in the inset for a better view. As expected, the accumulated free-volume fraction decreases drastically with increasing size of the test permeant. The accumulated free-volume fraction is related to the probability density of finding a cavity which can accommodate a spherical permeant with a vdW volume of V, $p(V, z)$, by

$$f(V,z) = \int_{V}^{\infty} p(V',z) \, dV'. \tag{6}$$

For $V = 0$, $f(V, z)$ gives the total free-volume fraction in the model bilayer. The total free-volume fraction obtained

by the extrapolation of the free-volume distribution to $V = 0$ is plotted in Fig. 6 versus position from the bilayer interface. The result is in contrast to the scaling theory which assumes a uniform profile for free-volume fraction (de Gennes, 1980; Milner et al., 1988), but in better agreement with a parabolic distribution as shown by the solid line in Fig. 6. The parabolic distribution can be derived from a self-consistent field theory (SCF) (Milner et al., 1988). Similar and related density profiles are also found from MD simulations of systems of end-grafted polymers (Murat and Grest, 1989a, 1989b). In our model bilayer, the total free-volume fraction varies from 0.30 in the highly ordered chain region to 0.49 in the center of the bilayer. The ratio of these two values is 0.61. The total free-volume fraction in the plateau region is close to those calculated in glassy poly(propylene) and poly(vinyl chloride), 0.31 and 0.32, in which the polymer chains are also highly ordered locally (Shah et al., 1989). The total free-volume fraction in bulk hydrocarbon liquids is 0.50 for n-pentane, 0.46 for n-octane, and 0.42 for n-hexadecane at 293 K (Bondi, 1954). Using temperature expansion coefficients (α) of 1.8×10^{-3}/K for n-pentane, 1.2×10^{-3}/K for n-octane, and 1.0×10^{-3}/K for n-hexadecane, which are evaluated from complied density-temperature data (American Institute of Physics Handbook, 1972; Boelhouwer, 1967), and an empirical thermodynamics relationship, $f = f_0 + \alpha(T - T_0)$, we estimate their total free-volume fractions at 323 K to be 0.56, 0.50, and 0.45, respectively. The total free-volume fraction in liquid n-octane estimated from the present MD simulation was $f = 0.58$. Considering various uncertainty in both simulation and experiment, especially the following two, the discrepancy from the value, 0.50, obtained from Bondi's data (Bondi, 1954) is not unreasonable: 1) the anisotropic interaction ignored in the present united-atom model may affect the hydrocarbon density at a given pressure and thereby change the total free-volume fraction (Toxvaerd, 1990) and 2) the difference of the methods used to estimate f. In Bondi's treat-
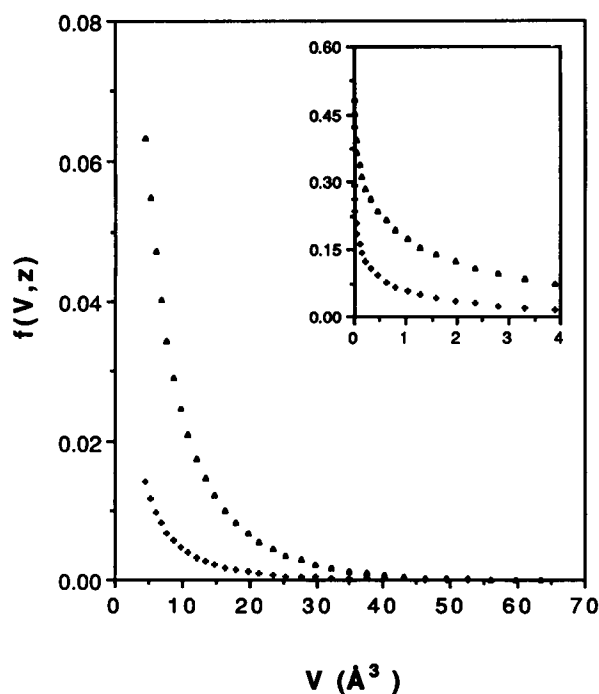

FIGURE 5 The distributions of the accumulated free-volume fraction, $f(V, z)$, at two different locations from the bilayer interface: $+$, $z = 1.50$ Å and $\triangle$, $z = 15.0$ Å, versus the vdW volume V of a test permeant.
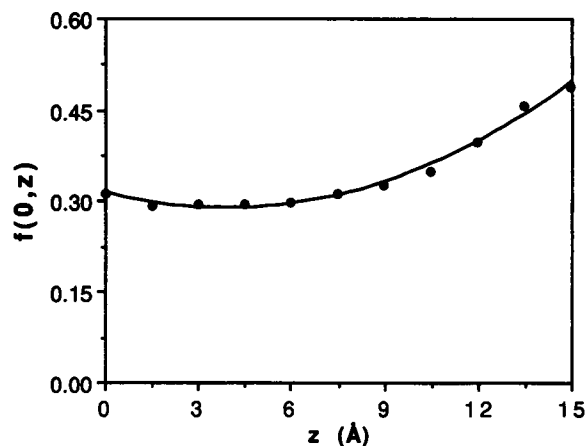

FIGURE 6 The total free-volume fraction, $f(0, z)$, obtained by extrapolating the distributions of the accumulated free-volume fraction to $V = 0.0$, versus distance from the interface.

ment, f was defined as $(V_T - V_W)/V_T$, where V_T is the macroscopic volume and V_W the volume of substance as calculated from the vdW dimension obtained by x-ray diffraction methods or by gas kinetic collision cross section. The f value is thus critically dependent on the accuracy of the experimental data obtained in or before the 1950s and the relationship between the vdW dimension and the L-J parameters, which unfortunately was not presented in the original paper.

The differentiation of Eq. 6 with respect to $-V$ yields the probability distribution for the free volume which can accommodate a spherical permeant of volume V, $p(V, z)$. Two representative profiles at $z = 1.50$ and 15.0 Å are displayed in Fig. 7 on a semilog scale. The rapid decline of the probability distributions with increasing size of small test permeants ($<\sim 1$ Å), as shown in the inset, indicates that there is a group of small free volume which composes the majority of the cavities in the bilayer and has a very narrow distribution with respect to the cavity size of the free volume. This group of free volume consists, in part, of dead spaces between neighboring chain segments when they are in contact with each other as in a lattice structure at 0 K. For example, a cavity formed by four contacting segments can accommodate a spherical permeant of $V = (\pi/6) [(r^2 + b_o^2)^{0.5} - r]^3 = 0.067$ Å^3, where $r (= 2.1$ Å$)$ is the vdW radius of a methylene group and $b_o (= 1.54$ Å$)$ is the bond length between adjacent methylene groups. Increased amplitude of vibration at an elevated temperature between adjacent segments due to intramolecular bonding broadens the cavity-size distributions but only within a small range since the displacements of atoms in vibration are small. It is also known as the fluc-

tuation or interstitial free volume (Bondi, 1954; Vrentas, 1977). Since this group of free volume has very small sizes and the energy exchange associated with redistribution of the interstitial free volume is very large, it is not effectively involved in most molecular transport processes. In support of this viewpoint is a substantial body of evidence in polymer systems that not all of the free volume participates in diffusion processes of solutes. Furthermore, its contribution to the cavity-size distributions becomes negligible for free volume available to spherical permeants with vdW volumes greater than approximately 4 Å^3, which is our main interest in the following analysis. It is also called effective free volume even though the boundary separating it from both dead volume and interstitial free volume can not be clearly defined.

As shown in Fig. 7, the probability distributions for the effective free volume fall off much slower with increasing size of the test permeant and fail to follow a single exponential decay. Model equations with one-, two-, and three-exponential components are utilized to fit the probability distributions for the effective free volume, which gives the MSC values (cf., the Monte Carlo Method section) of 2.4, 4.5, and 5.0, respectively, for the distribution at $z = 1.50$ Å. Similar results are obtained for the distributions at other locations in the bilayer. In addition, in the regression analysis using the model equation with three-exponential components, the pre-exponential factor for the third exponential term is always close to zero. Thus, it is concluded that a function with two exponential components

$$p(V, z) = p_1 e^{-V/V_1} + p_2 e^{-V/V_2} \qquad (7)$$

is best suited to describe the probability distributions for the effective free volume.

For a system of hard spheres in thermodynamic equilibrium, the principle of maximal entropy requires that the cavity-size distribution decreases exponentially with increasing size of the free volume (Cohen and Turnbull, 1959)

$$p(V, z) = p_0 e^{-V/V_0}. \qquad (8)$$

In fact, this functional form for free-volume distributions has been widely used to describe various transport processes. In contrast, our statistical analysis reveals the existence of two groups of effective free volume regardless of the local order. We have also analyzed the free-volume data for model polymers calculated by Shah et al. (1989), where the chain model with explicit hydrogen atoms is quite different from ours, and found that the distribution is also multiple exponential. Thus, the result seems to be independent of the chain model used and precise values of the L-J parameters. These observations suggest that the appearance of more than one exponential components in the free-volume distribution is a general phenomenon for systems consisting of polyatomic molecules with nonspherical shape.

The characteristic cavity sizes available to spherical permeants (V_1 and V_2) are presented in Fig. 8 as a function of distance from the interface. It is noted that V_1 varies only slightly across the bilayer interior with an average value of
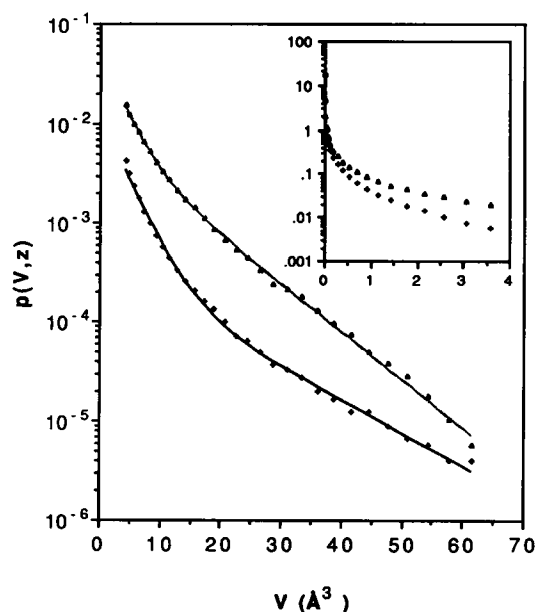

FIGURE 7   The probability distributions, $P(V, z)$, of finding a cavity size which can accommodate a spherical permeant with a vdW volume of V. The permeants are at two different locations in the bilayer interior: $+$, $z = 1.50$ Å and $\triangle$, $z = 15.0$ Å. The solid lines are from least-square fits using Eq. 7. The inset shows the distributions between $V = 0.0$ and 4.0 Å^3.
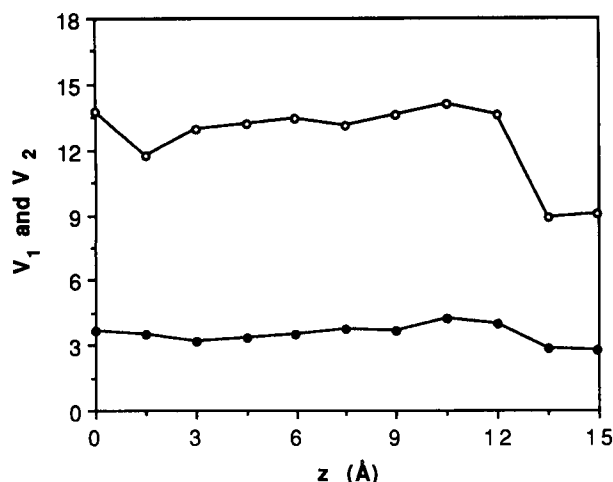
FIGURE 8   The characteristic cavity sizes, V_1 and V_2, obtained by fitting the free-volume distributions, $p(V, z)$, with Eq. 7, versus distance from the interface: ●, V_1; ○, V_2.

3.4 Å^3, whereas a large decrease in V_2 from the plateau value of 12.9 Å^3 in the highly ordered chain region to 9.0 Å^3 in the center of the bilayer is observed. The pre-exponential factors for these two groups of free volume, p_1 and p_2, change substantially from the plateau values of 0.012 and 0.00039 Å^{-3}, respectively, in the highly ordered chain region to 0.049 and 0.0067 Å^{-3} in the center of the bilayer as shown in Fig. 9. Here, the behavior essentially parallels that of the segmental order parameter. There is much more free volume in the
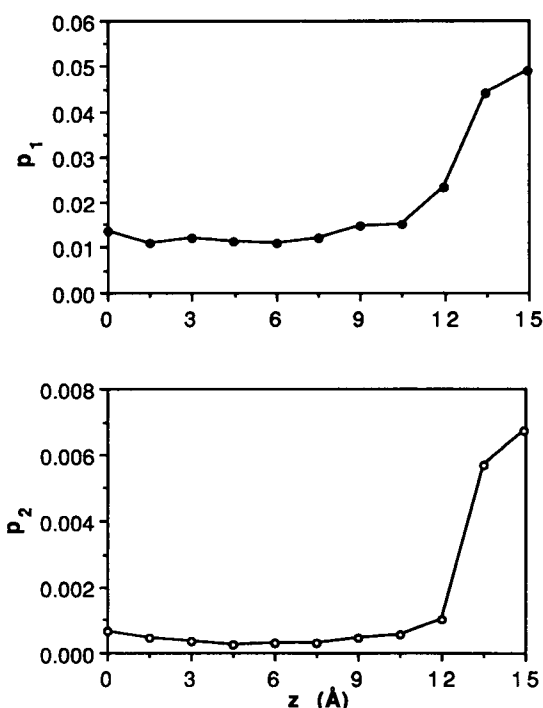

FIGURE 9   The pre-exponential constants, p_1 and p_2, obtained by fitting the free-volumes distributions with Eq. 7, versus distance from the interface: ●, p_1; ○, p_2.

center of the bilayer than in the highly ordered chain region, but the characteristic cavity size available to spherical permeants is somewhat smaller in the center of the bilayer than in the highly ordered chain region. Although the direct cause for the variation of the characteristic cavity sizes across the bilayer interior and the nature of these two groups of free volume are not fully understood, they appear to be associated with (a) the higher fluidity of chain segments in the center of the bilayer which makes large free volume more susceptible to being occupied by surrounding chain segments from both monolayers; (b) the overlap of adjacent segments in a chain molecule in the presence of covalent bonds; and (c) conformational transitions of chain molecules in the bilayer.

It is meaningful to discuss our simulation results either quantitatively or qualitatively in conjunction with available experimental data, even though the chemical compositions of the model and real lipid bilayers and other system conditions may not be identical. X-ray diffraction experiments on PC bilayers have shown characteristic electronic density dip in the center of the bilayers (McIntosh, 1980; McIntosh et al., 1980). Two free-volume properties may affect the observed density dip: the number of cavities and the mean cavity size. The density dip was previously attributed to two assumptions: 1) the richness of methyl groups in the center of the bilayers and 2) larger free volume is associated with terminal methyl groups (Gruen, 1985). The first assumption is consistent with the experimental finding that the ratios of methylene groups to methyl ends are inversely correlated with liquid hydrocarbon density (Flory et al., 1964; Orwoll and Flory, 1967), but the second assumption is in contrary with our simulation results, namely, the effective free volume in the center of the bilayer is, on the average, smaller than its counterpart in the highly ordered chain region. Thus, it is clear that the smaller number of cavities in the highly ordered chain region than that in the relatively disordered central region is primarily responsible for the density dip.

Applying the conventional free-volume theory (cf., Eq. 8) to the interpretation of experimental results on basal permeability across red cell membranes, Stein estimated the mean free volume in the barrier domain to be 14 Å^3 (Stein, 1986). Since most solutes used in Stein's study have vdW volumes considerably larger than V_1, the mean free volume obtained is thus an approximation of V_2. The closeness between the simulation and experimental values may come as a result of the cancellation of various factors affecting the observed transport permeability: (a) the presence of double bonds and protein macromolecules (even though some chemicals had been added to inhibit specific transport pathways due to the presence of these macromolecules) in red-cell bilayers may generate larger free volume; (b) the nonspherical permeants employed in the experiment may occupied smaller effective free volume when they penetrate through the membrane as suggested by our result in the following section that free volume is elongated in the bilayer; and (c) the lower temperature in the experimental system decreases the number of gauche defects, which may reduce the amount of large free volume in the membrane.

A study by Windrem et al. (Windrem and Plachy, 1980) found that the product of solubility and diffusion coefficients for molecular oxygen in phosphatidylcholine and other lipid bilayers in liquid-crystalline states depends strongly on the location at which oxygen interacts with a spin label, dox-ystearic acid. At 323 K and in DPPC bilayers, the ratio of the solubility-diffusion products at segmental positions C_{16} and C_5 is 1.5. In conform with the free-volume theories for molecular solubility and diffusion (Turnbull and Cohen, 1970; Schnitzer, 1988), the solubility-diffusion product at a given location z in the bilayer interior, $S(z)D(z)$, can be described by the equation

$$S(z)D(z) = C[p_1 V_1(V_1 + V)e^{-V/V_1} + p_2 V_2(V_2 + V)e^{-V/V_2}]$$
$$\times [p_1 e^{-V/V_1} + p_2 e^{-V/V_2}] \qquad (9)$$

where C is a proportionality factor independent of the co-ordinate z. Since the vdW radius for atomic oxygen (1.52 Å) is much larger than the bond length in molecular oxygen (0.66 Å) and the available free volume is largely determined by the short dimension of a permeant as most free volume is elongated (vida supra), the vdW volume for atomic oxygen is used in Eq. 9. An interpolation of the data in Figs. 8 and 9 using calculated average positions for C_{16} and C_5 gives the free-volume parameters in the corresponding positions. The ratio of the solubility-diffusion products is then estimated to be 6.8. The large discrepancy is probably associated with the perturbation, in the experimental system, of local free volume due to the presence of a relatively large probe group in the neighborhood of an oxygen molecule. The validity of the interpretation of spin relaxation mechanisms in the lipid bilayers is also subject to debate (Berner and Kivelson, 1979).

Mean cavity shape of free volume

The cavity-shape analysis is performed, as stated in the Monte Carlo Method section, by calculating the probability distribution of the direction at which the randomly selected permeant is in contact with one of the segments in the bilayer. The idea is that if a cavity is elongated, there is a higher probability for a test permeant to collide with a segment along the short dimension of the cavity. As the mean cavity shape approaches the spherical symmetry and in the limit of zero-size probe permeant, the probability density for the contact angle θ becomes, $\frac{1}{2}(\cos\theta_{i,1} - \cos\theta_{i,2})\Delta\theta^{-1}$, where $\theta_{i,1}$ and $\theta_{i,2}$ are the contact angles at the boundaries of the angle strip i. Fig. 10 a displays two representative distributions of the probability density, $P(\theta, V, z)$, as a function of the contact angle θ, where the free volumes is located at $z = 2.3$ and 15 Å from the interface, and the test permeant has a vdW volume of 6.6×10^{-5} Å^3. The hypothetical distribution, $P(\theta_i) = \frac{1}{2}(\cos\theta_{i,1} - \cos\theta_{i,2})\Delta\theta^{-1}$, is also plotted in the figure as a reference. In Fig. 10 b, the contact-angle distribution in the simulated bulk n-octane is displayed along with the hypothetical distribution. It is noted that the distributions in the center of the bilayer and in the n-octane liquid agree very closely with the hypothetical one, whereas the distribution in the highly ordered chain region is substantially narrower.
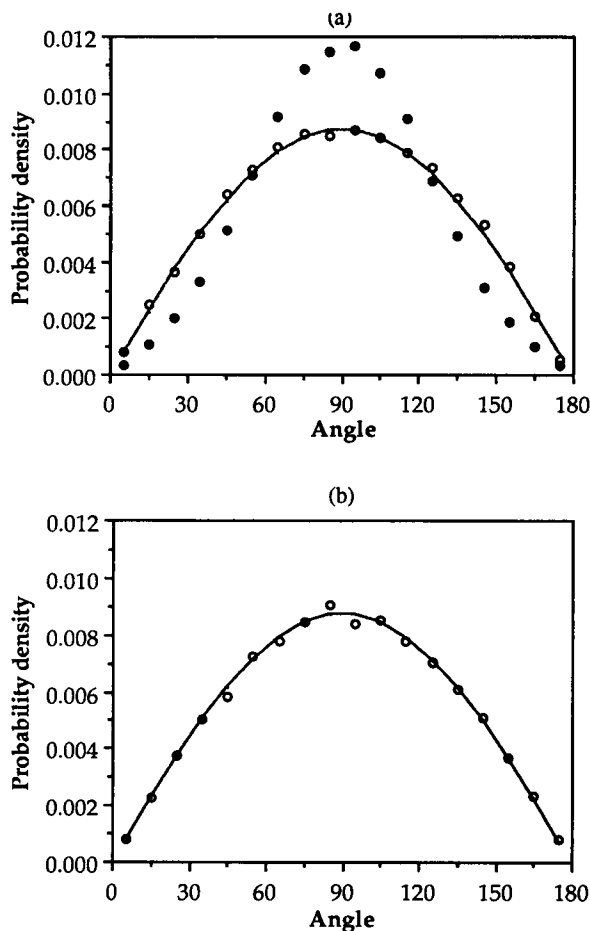

FIGURE 10　The contact-angle probability distributions, $P(\theta, V, z)$, as a function of the contact angle θ: (a) ●, at $z = 2.3$ Å and ○, at $z = 15$ Å from the interface; (b) ○, in n-octane liquid. The test permeant has a vdW volume of 6.6×10^{-5} Å^3. The solid lines in both figures are from the hypothetical distribution (Eq. A.2).

These results indicate that, on the average, the free volume in the center of the bilayer and in bulk n-octane is approximately spherical due to the random orientation of free volume, while the free volume in the highly ordered chain region is elongated with its long axis along the bilayer normal.

The facts that the contact-angle distributions are approximately symmetric about $\theta = 90°$ and the bilayer structure is statistically symmetric in the x-y plane suggest that the mean cavity shape of the free volume is an ellipsoid. The ellipticity of the mean cavity can be characterized more simply by the ratio between an arithmetic average of the probability densities at $\theta = 0$ and 180° and the probability density at $\theta = 90°$,

$$r(V, z) = \frac{[P(0°, V, z) + P(180°, V, z)]}{2P(90°, V, z)}. \qquad (10)$$

Fig. 11 presents two sets of data for $r(V, z)$ as a function of distance from the interface, in which the test permeants have vdW volumes of 6.6×10^{-5} and 9.7 Å^3, respectively. As noted, the ratio has plateau values of 0.031 and 0.067 for $V = 6.6 \times 10^{-5}$ and 9.7 Å^3, respectively, in the highly
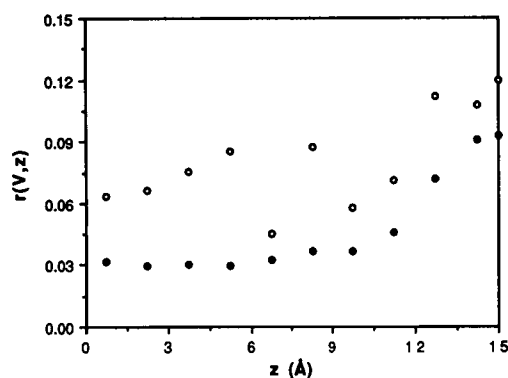
FIGURE 11   The ellipticity ratio, $r(V, z)$, versus distance from the interface: ● and ○ are for the test permeants with vdw volumes of 6.6×10^{-5} and 9.7 Å^3, respectively.

ordered chain region and increases to 0.093 and 0.12, respectively, at the mid-plane. The greater fluctuation of the data points for the larger test permeant is due to the very limited number of large cavities sampled. The significantly smaller ratio for cavities available to the smaller permeant implies that small free volume is more elongated than large free volume. A similar phenomenon was observed in a MD simulation of polymer liquid and glass, where the reduced surface-to-volume ratio for the free volume decreases with increasing cavity size (Rigby and Roe, 1990). The nonsphericity of free volume in the highly ordered region also implies that the true mean cavity sizes for the two groups of effective free volume are larger than V_1 and V_2 in that region.

Conformational structure

In the rotational isomeric state approximation (Volkenstein, 1963), torsional motion of a dihedral angle is characterized by three discrete states, trans and ±gauche. Different combinations of these conformational states among neighboring chain molecules can create cavities of different sizes. Thus, it is important to investigate the conformational structure in the model bilayer. Fig. 12 presents the probability distribution of finding a gauche state for the nth dihedral angle in the
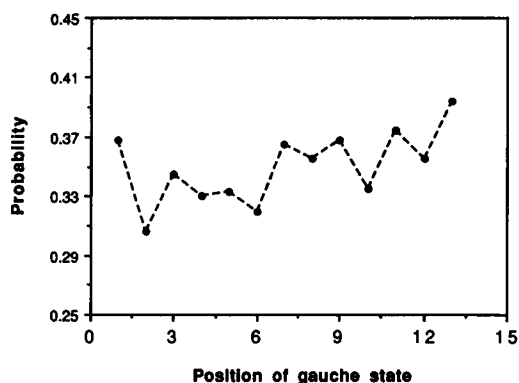

FIGURE 12   The probability distribution of the occurrence of a gauche state versus the position of the gauche state.

linkage, C_n-C_{n+1}-C_{n+2}-C_{n+3}. An odd-even effect is observed as did in other bilayer assemblies (van der Ploeg and Berendsen, 1983; Egberts and Berendsen, 1988). The probabilities are, on the average, 0.32 in the highly ordered chain region and 0.39 at the tail of the chain. The energy gap between a gauche and trans rotamer is 700 cal/mol in the Rychaert-Bellemans potential, which corresponds to a probability of 0.40 for the occurrence of a gauche state at an isolated dihedral angle at 323 K. It is then noted that gauche states are severely suppressed in the highly ordered chain region.

Table 2 lists the average numbers of various conformational sequences in a chain molecule along with those predicted from a statistically independent model. This model is defined as a free chain in vacuum with torsional angles independent of each other and driven by the R-B potential. The combinations of two gauches, g_+tg_- and g_-tg_+, are known as kinks and g_+tttg_- and g_-tttg_+ as jogs. These defects are of special interest because of their roles in cooperative conformational transitions as in the Crank shaft-like models (Skolnick and Helfand, 1980; Helfand, 1971; Helfand, 1985) and in the creation of relatively large free volume (Träuble, 1971). Kinks and jogs are energetically preferred over other gauche defects in a lipid bilayer because they preserve the overall orientation of the chain molecule and thereby have a minimal disturbance to the compact structure of the lipid bilayer. However, a large increase in numbers of these defects would result in a decrease in system entropy. Thus, the conformational structure observed should reflect a subtle balance between these two factors. The average number of kinks in a chain molecule is 0.76, larger than the prediction from the independent model, 0.53, while there is no difference in the average number of jogs per chain molecule between the simulation result and the model prediction. The fact that most of the chain molecules in the bilayer have one kink sequence suggests the possible importance of cooperative motions in the free-volume distributions.

An isolated gauche state is defined, in this work, as the gauche state which does not belong to any other type of conformational sequences as specified in Table 2. An isolated gauche state may cause a large defection of the chain orientation, and thus, may not be favored in a lipid bilayer, especially near the head group. The average number of isolated gauches per chain molecule is 1.41, much smaller than the average number of gauche states available. The occurrence of gauche pairs of the same sign, $g_\pm g_\pm$, is less frequent

TABLE 2   Average numbers of conformational sequences per chain molecule

Sequences	MD simulation	Independent model
Isolated gauche	1.41	
Kinks	0.76	0.53
Jogs	0.16	0.16
$g_\pm g_\pm$	0.54	0.97
$g_\pm g_\pm g_\pm$	0.14	0.18
$g_\pm g_\pm g_\pm g_\pm$	0.036	0.036
$g_+ g_-$ and $g_- g_+$	0.18	0.97

than predicted from the independent model. Examination of a molecular model shows that the two terminal methylene groups in a $g_{\pm}g_{\pm}$ sequence are at a distance of 3.57 Å from each other, which corresponds to a L-J interaction energy of 0.73 kJ/mole. This repulsive energy accounts for about 40% of the decrease in the average number of such sequences at 323 K. The average numbers of multiple *gauche* states of the same sign, $(g_+)_n$ and $(g_-)_n$, where $n = 3$ and 4, are also calculated and found to be more consistent with the prediction from the independent model.

As noted in Table 2, the unfavorable sequences, g_+g_- and g_-g_+ can be easily detected in the bilayer structure even though at a much smaller probability than predicted from the independent model. These conformational defects are severely suppressed, because of the strong steric repulsion between the segments separated by four C-C bonds, also known as the pentane effect (Pitzer, 1940). They have been assumed to be forbidden and neglected in many conformational analyses. Nevertheless, it has been suggested by Flory and others (Flory, 1989) that the severe steric overlap for the *gauche* pairs of opposite sign in a chain molecule can be alleviated by moving away from the angles, $\pm 120°$. Two shallow energy minima were identified at $\phi = \pm 115$ and $\pm 77°$, having an energy of 3.2 kcal/mol above the *trans* pair state (tt) (Flory, 1989). It corresponds to a probability of 0.0071 for the occurrence of either g_+g_- or g_-g_+, or an average of 0.17 such defects per chain molecule, which is in close agreement with our simulation result, 0.18. As another evidence, our simulation shows that the *gauche* pairs of the opposite sign have, on the average, their dihedral angles at $\phi = \pm 109$ and $\pm 79°$.

CONCLUSIONS AND COMMENTS

In this work, a novel combined method of the molecular dynamics and Monte Carlo simulations is developed to calculate the free-volume distributions across the model lipid bilayer and a new method based on the contact-angle distribution is developed to describe quantitatively mean cavity geometry. Although approximate models were employed in the MD simulation, some structural features observed in experiment, including the segmental order parameter, surface density and mean cavity volume, were reproduced either quantitatively or qualitatively. These facts along with the fact that the potential used for chain molecules has been tested in numerous previous studies imply that the basic ingredients are contained in our model and that special details not included in out model likely do not alter the main picture and the qualitative but important observations obtained in this work. Namely, 1) the probability distributions for the effective free volume at different locations in the bilayer are found to have two exponential components. 2) The ordering of alkyl chains in the bilayer decreases the fraction of both free-volume components, but the characteristic cavity sizes available to spherical permeants are smaller in the relatively disordered central region than in the highly ordered chain region. The relative scarce of free volume in the highly or-

dered chain region reduces both solubility and diffusivity of permeants in that region as demonstrated by the ratio of solubility-diffusion products for molecular oxygen. Thus, it provides an effective barrier to transport processes of permeants, a result in consistence with our recent experiments on functional group contributions to permeability of *p*-toluic acid and α-position derivatives (Xiang et al., 1992). 3) Our preliminary results reveal that the mean shape of free volume in the bilayer is an ellipsoid. The ellipticity of the free volume increases with distance from the interface approaching the limiting value for spherical cavity in the center of the bilayer.

The local order and conformational structures are also analyzed. Some salient features of our findings are as follows: (*a*) both overall and internal motions of the chain molecules have comparable contributions to the disorder in the bilayer and the coupling between these two motional modes appears to be responsible for the plateau order parameter along the chain; (*b*) the kink defects have increased probability than predicted from the independent model; (*c*) the *gauche* pairs of the opposite sign, which have been known to be highly unfavorable due to excluded volume interactions (Scott, 1975), can be easily detected in the bilayer structure. This is attributed to the fact that in the bilayer, a dihedral angle can assume values other than 0 and $\pm 120°$, which alleviates substantially the strong steric expulsion.

The lack of explicit water and head groups may affect the free-volume in the following ways: 1) the chemical nature of head groups and the degree of hydration can change the surface density of lipid chains. In our simulation, the surface density was varied to fit the experimental data. Thus, this effect is largely accounted for. 2) the penetration of external molecules such as water, driven by a configurational entropy (Wang et al., 1993), is known to perturb the local chain conformation and decrease the degree of compact packing of chain molecules in the bilayer. This effect is expected to increase local free-volume fraction. But this effect, like the effect of anchoring two chains to a head group, is only significant near the polar head group region as experimental studies by the author (not published) and others indicate that the partition coefficient for water between a nonpolar hydrocarbon solvent and water phases is on the order of 10^{-5} (molarity ratio).

More studies are under progress to 1) establish a quantitative relationship between the contact-angle distribution and the actual topology of free volume; 2) to examine the effects of intermolecular anisotropic interaction on lipid bilayer structure; 3) to explore the effects of surface density and temperature on the free-volume distributions; and 4) to understand the nature and the dynamic relaxation of effective free volume and their correlation with conformational structure of chain molecules in the bilayers.

APPENDIX

For a spherical cavity as shown in Fig. 13, the surface area of a spherical sector between θ_1 and θ_2, with which a test permeant is in contact, can be
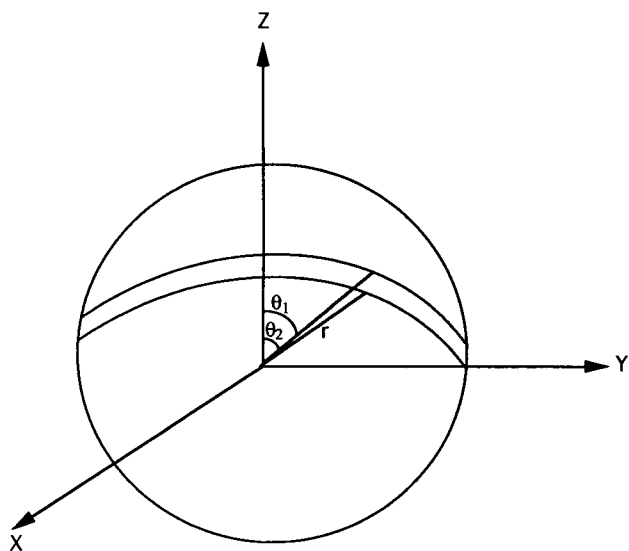
FIGURE 13   An illustration of a spherical cavity and a selected spherical sector whose surface area is proportional to the probability for the contact angle between θ_1 and θ_2.

expressed as

$$S(\theta_1, \theta_2) = 2\pi r^2 \int_{\theta_1}^{\theta_2} \sin \theta \, d\theta = 2\pi r^2 [\cos \theta_1 - \cos \theta_2]. \quad (11)$$

Since the surface area is sampled uniformly, the probability for the contact angle at $\theta = \theta_1 + \frac{1}{2}(\theta_2 - \theta_1)]$ is obtained by dividing the above equation by the total surface area of the sphere, $4\pi r^2$, which gives

$$P(\theta) = \frac{1}{2}(\cos \theta_1 - \cos \theta_2). \quad (12)$$

As noted, the distribution is independent of the cavity size.

ACKNOWLEDGMENTS

REFERENCES

Allen, M. P., and D. J. Tildesley. 1989. Computer simulation of liquids. Oxford University Press, New York. 78–82.

Andrea, T. A., W. C. Swope, and H. C. Anderson. 1983. The role of long ranged forces in determining the structure and properties of liquid water. *J. Chem. Phys.* 79:4576–4584.

Bareman, J. P., and M. L. Klein. 1990. Collective tilt behavior in dense, substrate-supported monolayers of long-chain molecules: a molecular dynamics study. *J. Phys. Chem.* 94:5202–5205.

Berner, B., and D. Kivelson. 1979. The electron spin resonance line width method for measuring diffusion. A critique. *J. Phys. Chem.* 83:1406–1412.

Biswas, A., and B. L. Schurmann. 1991. Molecular dynamics simulation of a dense model bilayer of chain molecules with fixed head groups. *J. Chem. Phys.* 95:5377–5386.

Boelhouwer, J. W. M., 1967. Sound velocities in and adiabatic compressibilities of liquid alkanes at various temperatures and pressures. *Physica.* 34:484–492.

Bondi, A. 1954. Free volumes and free rotation in simple liquids and liquid saturated hydrocarbons. *J. Phys. Chem.* 58:929–939.

Cohen, M. H., and D. Turnbull. 1959. Molecular transport in liquids and glasses. *J. Chem. Phys.* 31:1164–1168.

Gennes, P. G. 1980. Conformations of polymers attached to an interface. *Macromolecules.* 13:1069–1075.

Loof, H., S. C. Harvey, J. P. Segrest, and R. W. Pastor. 1991. Mean field stochastic boundary molecular dynamics simulation of a phospholipid in a membrane. *Biochemistry.* 30:2099–2113.

Eiteman, M. A., and J. L. Gainer. 1989. The effect of free-volume changes on partitioning in magnesium sulfate-poly(ethylene glycol) aqueous two-phase systems. *Biochim. Biophys. Acta.* 992:125–127.

Egberts, E., and H. J. C. Berendesen. 1988. Molecular dynamics simulation of a smectic liquid crystal with atomic detail. *J. Chem. Phys.* 89:3718–3732.

Ferrarini, A., P. L. Nordio, G. J. Moro, R. H. Crepeau, and J. H. Freed. 1989. A theoretical model of phospholipid dynamics in membranes. *J. Chem. Phys.* 91:5707–5721.

Fixman, M. 1974. Classical statistical mechanics of constraints: a theorem and application to polymers. *Proc. Natl. Acad. Sci. USA.* 71:3050–3053.

Flory, P. J. 1989. Statistical mechanics of chain molecules. Oxford University Press, New York. and references within.

Flory, P. J., R. A. Orwoll, and A. Vrij. 1964. Statistical thermodynamics of chain molecule liquids. I. An equation of state for normal paraffin hydrocarbons. *J. Am. Chem. Soc.* 86:3507–3514.

Gray, D. E., editor. American Institute of Physics Handbook. 1972. McGraw-Hill Book Co., New York. 2–181.

Griffith, O. H., P. J. Dehlinger, and S. P. Van. 1974. Shape of the hydrophobic barrier of phospholipid bilayers. *J. Membr. Biol.* 15:159–192.

Gruen, D. W. R. 1985. A model for the chains in amphiphilic aggregates. 1. Comparison with a molecular dynamics simulation of a bilayer. *J. Phys. Chem.* 89:146–153.

Helfand, E. 1971. Theory of the kinetics of conformational transitions in polymers. *J. Chem. Phys.* 54:4651–4661.

Helfand, E.. 1979. Flexible vs rigid constraints in statistical mechanics. *J. Chem. Phys.* 71:5000–5007.

Helfand, E. 1985. Dynamics of conformational transitions in polymers. *Science (Wash. DC).* 226:647–650.

Helfand, E., Z. R. Wasserman, and T. A. Weber. 1980. Brownian dynamics study of polymer conformational transitions. *Macromolecules.* 13:526–533.

Hubbell, W. L., and H. M. MaConnell. 1971. Molecular motion in spin-labeled phospholipids and membranes. *J. Am. Chem. Soc.* 93:314–326.

Jacobs, R. E., B. S. Hudson, and H. C. Anderson. 1977. A theory of phase transitions and phase diagrams for one- and two-component phospholipid bilayers. *Biochemistry.* 16:4349–4359.

Jorgensen, W. L., and J. Tirado-Rives. 1988. The OPLS potential functions for proteins. Energy minimizations for crystals of cyclic peptides and Crambin. *J. Am. Chem. Soc.* 110:1657–1666.

Karaborni, S., and S. Toxvaerd. 1992. Molecular dynamics simulations of Langmuir monolayers: a study of structure and thermodynamics. *J. Chem. Phys.* 96:5505–5515.

Liu, F., W. J. Horton, C. L. Mayne, T.-X. Xiang, and D. M. Grant. 1992. Molecular dynamics of 1-decanol in solution studied by NMR coupled relaxation and stochastic dynamics simulations. *J. Am. Chem. Soc.* 114:5281–5294.

McIntosh, T. J., S. A. Simon, and R. C. MacDonald. 1980. The organization of n-alkanes in lipid bilayers. *Biochim. Biophys. Acta.* 597:445–463.

McIntosh, T. J. 1980. Differences in hydrocarbon chain tilt between hydrated phosphatidylethanolamine and phosphatidylcholine bilayers. A molecular packing model. *Biophys. J.* 29:237–246.

Milik, M., A. Kolinski, and J. Skolnick. 1990. Monte Carlo dynamics of a dense system of chain molecules constrained to lie near an interface. A simplified membrane model. *J. Chem. Phys.* 93:4440–4446.

Milik, M., J. Skolnick, and A. Kolinski. 1992. Monte Carlo studies of an idealized model of a lipid-water system. *J. Phys. Chem.* 96:4015–4022.

Milner, S. T., T. A. Witten, and M. E. Cates. 1988. Theory of the grafted polymer brush. *Macromolecules.* 21:2610–2619. and references within.

Murat, M., and G. S. Grest. 1989a. Interaction between grafted polymeric brushes: a molecular-dynamics study. *Phys. Rev. Lett.* 63:1074–1077.

Murat, M., and G. S. Grest. 1989b. Structure of a grafted polymer brush: a molecular dynamics simulation. *Macromolecules.* 22:4054–4059.

Orwoll, R. A., and P. J. Flory. 1967. Equation-of-state parameters for normal alkanes. Correlation with chain length. *J. Am. Chem. Soc.* 89:6814–6822.

Pastor, R. W., R. M. Venable, and M. Karplus. 1988a. Brownian dynamics simulation of a lipid chain in a membrane bilayer. *J. Chem. Phys.* 89: 1112–1127.

Pastor, R. W., R. M. Venable, M. Karplus, and A. Szabo. 1988b. A simulation based model of NMR T_1 relaxation in lipid bilayer vesicles. *J. Chem. Phys.* 89:1128–1140.

Pastor, R. W., R. M. Venable, and M. Karplus. 1991. Model for the structure of the lipid bilayer. *Proc. Natl. Acad. Sci. USA.* 88:892–896.

Peterson, N. O., and S. I. Chan, 1977., More on the motional state of lipid bilayer membranes: interpretation of order parameters obtained from nuclear magnetic resonance experiments. *Biochemistry.* 16:2657–2667.

Pitzer, K. S. 1940. The vibration frequencies and thermodynamic functions of long chain hydrocarbons. *J. Chem. Phys.* 8:711–720.

Rand, R. P., and V. A. Parsegain. 1989. Hydration forces between phospholipid bilayers. *Biochim. Biophys. Acta.* 988:351–376.

Rigby, D., and R. J. Roe. 1990. Molecular dynamics simulation of polymer liquid and glass. 4. Free-volume distribution. *Macromolecules.* 23:5312–5319.

Rychaert, J. P., and A. Bellemans. 1975. Molecular dynamics of liquid *n*-butane near its boiling point. *Chem. Phys. Lett.* 30:123–125.

Schindler, H., and J. Seelig. 1975. Deuterium order parameters in relation to thermodynamic properties of a phospholipid bilayers. A statistical mechanical interpretation. *Biochemistry.* 14:2283–2287.

Schnitzer, J. E. 1988. Analysis of steric partition behavior of molecules in membranes using statistical physics. Application to gel chromatography and electrophoresis. *Biophys. J.* 54:1065–1076.

Scott, J. H. L. 1975. A theoretical model for lipid monolayer phase transitions. *Biochim. Biophys. Acta.* 406:329–346.

Scott, R. A., and H. A. Scheraga. 1966. Conformational analysis of macromolecules. II. The rotational isomeric states of normal hydrocarbons. *J. Chem. Phys.* 44:3054–3069.

Seelig, A., and J. Seelig. 1974. The dynamics structure of fatty acyl chains in a phospholipid bilayer measured by deuterium magnetic resonance. *Biochemistry.* 13:4839–4845.

Seelig, J., and W. Niederberger. 1974. Two pictures of a lipid bilayer. A comparison between deuterium label and spin-label experiments. *Biochemistry.* 13:1585–1588.

Shah, V. M., S. A. Stern, and P. J. Ludovice. 1989. Estimation of the free volume in polymers by means of a Monte Carlo technique. *Macromolecules.* 22:4660–4662.

Skolnick, J., and E. Helfand. 1980. Kinetics of conformational transitions in chain molecules. *J. Chem. Phys.* 72:5489–5500.

Stein, W. D. 1986. Transport and diffusion across cell membranes. Academic Press, New York.

Toxvaerd, S., 1990. Molecular dynamics calculation of the equation of state of alkanes. *J. Chem. Phys.* 93:4290–4295.

Träuble, H. 1971. The movement of molecules across lipid membranes: a molecular theory. *J. Membr. Biol.* 4:193–208.

Turnbull, D., and M. H. Cohen. 1970. On the free-volume model of the liquid-glass transition. *J. Chem. Phys.* 52:3038–3041.

der Ploeg, P. and H. J. C. Berendsen. 1982. Molecular dynamics simulation of a bilayer membrane. *J. Chem. Phys.* 76:3271–3276.

der Ploeg, P., and H. J. C. Berendsen. 1983. Molecular dynamics of a bilayer membrane. *Mol. Phys.* 49:233–248.

Vaz, N. A. P., J. W. Doane, and M. E. Neubert. 1979. Polymorphism in a lamellar liquid-crystal bilayer system. *Phys. Rev. Lett.* 42:1406–1409.

Vaz, W. L. C., R. M. Clegg, and D. Hallmann. 1985. Translational diffusion of lipids in liquid crystalline phase phosphatidylcholine multibilayers. A comparison of experiment with theory. *Biochemistry.* 24:781–786.

Volkenstein, M. V. 1963. Configurational statistics of polymeric chains. Interscience, New York.

Vrentas, J. S. 1977. Diffusion in polymer-solvent systems. I. Reexamination of the free-volume theory. *J. Polym. Sci. Polym. Phys. Ed.* 15:403–416.

Walter, A., and J. Gutknecht. 1986. Permeability of small nonelectrolytes through lipid bilayer membranes. *J. Membr. Biol.* 90:207–217.

Wang, D.-C., T. F. Taraschi, E. Rubin, and N. Janes, 1993. Configurational entropy is the driving force of ethanol action on membrane architecture, *Biochim. Biophys. Acta.* 1145:141–148.

Weiner, S. J., P. A. Kollman, D. A. Case, U. C. Singh, C. Ghio, G. Alagona, J. S. Profeta, and P. Weiner. 1984. A new force field for molecular mechanical simulation of nucleic acids and proteins. *J. Am. Chem. Soc.* 106:765–784.

Windrem, D. A., and W. Z. Plachy. 1980. The diffusion-solubility of oxygen in lipid bilayers. *Biochim. Biophys. Acta.* 600:655–665.

Woller, P. B., and E. W. Garbisch, Jr. 1972. The conformational analysis of *n*-butane. *J. Am. Chem. Soc.* 94:5310–5314.

Xiang, T.-X., F. Liu, and D. M. Grant. 1991. Stochastic dynamics of *n*-nonane and related molecules in solution compared with nuclear magnetic resonance coupled relaxation times. *J. Chem. Phys.* 95:7576–7590.

Xiang, T.-X., X. Chen, and B. D. Anderson. 1992. Transport methods for probing the barrier domain of lipid bilayer membranes. *Biophys. J.* 63: 78–88.